Effects of atmospheric stratification and jet position on the properties of early aircraft contrails

Pierre Saulgeot[*] and Vincent Brion[†]
DAAA, ONERA, Université Paris-Saclay, F-92190 Meudon, France

Nicolas Bonne[‡]
DMPE, ONERA, Université Paris-Saclay, F-91123 Palaiseau, France

Emmanuel Dormy[§]
Département de Mathématiques et Applications, UMR-8553, École Normale Supérieure, CNRS, 75005 Paris, France

Laurent Jacquin[¶]
DSG, ONERA, Université Paris-Saclay, F-91123 Palaiseau, France

(Received 10 March 2023; accepted 12 October 2023; published 30 November 2023)

The net impact of aircraft contrails on global climate change is a matter of controversy today. Among the many parameters potentially influencing this issue, the role played by the aircraft wake has received only little attention so far. Yet the interaction between the engine exhaust jets causing these contrails and the aircraft wake can lead to modifications in the altitude of the contrails on the order of hundreds of meters. This change in altitude heavily influences the net impact of contrails to global climate change, since it affects the ambient temperature and thereby the ice content and the radiative properties of these contrails. The wake entrainment supporting these effects basically depends on the relative positioning of the jet with respect to the tip vortices and on the buoyant forces associated with atmospheric stratification. Here we focus on these two parameters by running a large number of two-dimensional simulations of the flow from the aftermath of the jet turbulent diffusion, vortex roll-up, and initial ice formation up to the vortex destabilization stage, for a range of values of the vortex based normalization of the Brunt-Väisälä frequency and the jet to wing span ratio. The very near wake dynamics are not simulated and instead replaced by an analytical description for the vortex, the jet, and the ice plume. Ice water content is determined from the offset to ice saturation, given prescribed ambient conditions. The jet lateral spacing is considered in the range from fuselage to wing tip. The potential radiative impact of the early wake is calculated using the total extinction induced by the ice plume. The results are indicative of the impact of older contrail cirrus clouds, the largest proportion in the whole contrail radiative impact. The parametric mapping (stratification, jet spacing) highlights the important role played by the jet position on the opacity of early contrails, for regular stratification levels. In particular, a jet located closer to the wing tip

[*]pierre.saulgeot@onera.fr
[†]vincent.brion@onera.fr
[‡]nicolas.bonne@onera.fr
[§]emmanuel.dormy@ens.fr; https://www.math.ens.fr/~dormy.
[¶]laurent.jacquin@onera.fr

results in contrails located at lower altitudes and reduced optical thickness, suggesting that jet positioning could be an interesting mean of contrail mitigation.

DOI: 10.1103/PhysRevFluids.8.114702

I. INTRODUCTION

Civil aircraft contrails are an increasingly troublesome problem due to their potentially high impact on the aviation radiation budget. In supersaturated regions of the atmosphere, they can degenerate from initial line contrails into high-level cirrus clouds and last several hours. A recent study from [1] suggests that the impact of contrails on climate change could be larger than that of the release of CO_2 by the worldwide aircraft fleet: the radiative forcing caused by contrails could account for more than half of the radiative forcing of civil aviation whereas CO_2 one-third. However, these estimates remain very uncertain, with an uncertainty in the range 30% to 170%.

Contrails form under conditions of pressure, temperature, and humidity that are often encountered at cruise altitude. For example, at an altitude of 11000 m, the standard pressure and temperature are 250 hPa and 217 K, respectively, and the homogeneous nucleation threshold of water is about $RH_i \approx 170\%$. Aircraft engine exhaust contains additional water vapor compared to ambient air, typically 1.23 kg per kilogram of fuel burnt (called the emission index, hereafter denoted EI). This moist air, initially warm at the jet exit, cools very rapidly as it mixes with cold ambient air due to turbulent diffusion at the jet interface. During this mixing, air can reach conditions of temperature and moisture that are above the saturation curve of liquid or solid water. A simple model of these effects is implemented in the Schmidt-Appleman criterion [2], in which the exhaust flow follows an isobaric dilution from its thermodynamic state $(T_{\text{en}}, p_{v,\text{en}})$ at the exit of the engines to that of the atmosphere $(T_{\text{atm}}, p_{v,\text{atm}})$, where p_v denotes vapor pressure. The trajectory of the exhaust gases in the (T, p_v) plane is then a straight line. In order to predict contrail formation and persistence, this line can be compared to the saturation curves of liquid water (for an appearance criterion) and ice (for a persistence criterion [3]). However, the formation of ice in the aircraft wake cannot be described only by this thermodynamic reasoning. The complete picture requires microphysical phenomena that are not fully understood at the moment, but, for instance, condensation on soot from kerosene combustion seems to be the dominant factor for current jet engines. At present, sustainable aviation fuels (SAFs) as well as hydrogen are being investigated to reduce CO_2 emission. These alternative fuels have different EI and will produce a different mixture of soot and other aerosols that act as ice-nucleating particles. More importantly, the Schmidt-Appleman dilution model does not account for changes in atmospheric conditions around the jet plume induced by its interaction with the descending aircraft wake.

The interaction between the wake and the exhaust plume is generally divided into five phases [4–6]: the *jet phase*, the *deflection phase*, the *vortex phase*, the *dissipation phase*, and the *diffusion phase*. We describe them thereafter. Overall it is useful to have in mind that the aircraft wake is dynamically active until the *dissipation phase*, and that in the *diffusion phase*, the wake has lost all its momentum and the plume evolves under atmospheric effects only. During the *jet phase*, the dynamics of the engine exhaust jets and the wake are almost independent. Atmospheric stratification has therefore no influence on the evolution of the jet, due to its small size and the fact that its evolution is perpendicular to the density gradient. The jet dynamics main driver is the instability of the jet shear layer, which causes the main aspect of its development, that is, the jet diffusion in the radial direction and the mixing with the surrounding air. The vorticity sheet coming from the different wings of the airplane rolls up in a vortex wake [7], and the engine jets undergo isobaric dilution and strong turbulent diffusion, owing to the velocity difference at the jet periphery (roughly 200 ms^{-1} initially; see Table I, which presents the vortex and engine jet data for a typical aircraft). Condensation of water vapor occurs during this phase, if any. The possible sublimation of the ice crystals takes place during the following phases [8]. The *deflection phase* corresponds to the moment

TABLE I. Typical aircraft data taking the example of an A330 jetliner.

Wingspan b (m)	64.0
Jet engine separation b_{jet}/b	33%
Vortex circulation Γ_0 ($\text{m}^2\,\text{s}^{-1}$)	400
Aircraft flight velocity U_0 (ms^{-1})	250
Jet engine speed U_{en} (ms^{-1})	480
Ambient temperature T_0 (K)	217
Jet engine temperature T_{en} (K)	580
Jet engine exit diameter $D(x_{\text{out}})$ (m)	0.6

when the axial and transverse moments of the plume have the same order of magnitude. At this stage the interaction between the engine exhaust jets and the wake can no longer be neglected. This phase occurs in a zone between 1 and 10 wingspans behind the aircraft [4], depending on the aircraft type and on the lateral position of the engines. Although it has been the subject of experimental studies ([9,10]), this phase is often neglected in numerical studies ([11–14]) because of its complexity and high computational cost. The *vortex phase* begins when the specific dynamics of the jets becomes negligible [9,15]. During this phase, the engine plumes are dragged by the wake. An order of magnitude of the thresholds between these different phases (*jet*, *deflection*, and *vortex*) is obtained by the ratio R_3 introduced in [4] and recalled later in Sec. II A: $R_3 \gg 1$ during the jet phase (the vortex induction on the jet is negligible compared to the jet dynamics), $R_3(x_{\text{jet}}) \sim 1$ during the deflection phase (the vortex induction and the jet dynamics have the same order of magnitude), and $R_3 \ll 1$ during the vortex phase (the vortex induction on the jet is dominant compared to the jet dynamics). Beyond this approximate distance, the evolution of the jet is mostly dictated by the effect of entrainment by the vortex flow. At such distances behind the aircraft, it is necessary to mention that the vortex wake emanating from the wing has mostly rolled up into two trailing vortices that are close to axisymmetry (see [10], Fig. 5 of [16,17]). The vortices are characterized by their radius r_0 and circulation Γ_0, the latter being proportional to the ratio of the aircraft weight to the initial vortex spacing b_0. Their natural motion is a descent at constant speed W_0 caused by mutual induction. The value of W_0 can be estimated using a point vortex model following

$$W_0 \simeq \frac{\Gamma_0}{2\pi b_0}. \tag{1}$$

The vortex dipole has a lifetime of a few minutes before the onset of 3D instabilities that lead to its destruction: this is the *dissipation phase*. According to [18] the maximum lifetime of such a vortex pair is about five to six characteristic time units τ_0, which is defined as

$$\tau_0 = \frac{b_0}{W_0} = \frac{2\pi b_0^2}{\Gamma_0}. \tag{2}$$

This lifetime corresponds to a time of 198 to 236 s for the aircraft described in Table I, or a distance between 50 and 60 km behind the aircraft. At flight altitude, while low residual turbulence is generally expected, high levels can still be encountered in jet streams or cumuliform clouds. The level of external turbulence drives the time required for the loss of coherence of the wake vortices [19,20]. Lewellen's simulations [21], consisting of 3D LES of the vortex and dissipation phases of the wake of two aircraft (with synthetic turbulence), show 2D wake behavior up to times between 5 and 6 τ_0. The subsequent onset of Crow instability then leads to 3D dynamics only from this point onwards. The *diffusion phase* starts after that stage, when the wake has lost all its momentum and the plume becomes fully governed by the dynamics of the atmosphere.

This study focuses on the *vortex phase*. During this phase, atmospheric stratification can strongly modify the behavior of the wake. The vertical movement of the wake creates buoyant forces upon it that alter its descent and shape. This evolution depends at first order on the product of the

Brunt-Väisälä frequency and wake timescale τ_0. Typical values range between 0.1 (e.g., fully loaded B737 with weak stratification) and 1.8 (e.g., empty A330 with strong stratification). In a highly stratified atmosphere, the downward motion of the wake is overwhelmed by buoyancy, causing the wake to stagnate at flight altitude. Otherwise, the wake has a downward motion whose velocity and maximum height depend on the level of stratification [22]. Wake descent creates a density gradient at the edge of the Kelvin oval that causes the formation of additional vorticity by baroclinity [23]. It is called secondary, or baroclinic, vorticity. It is of the opposite sign to the vorticity present in the core of the nearest vortex, which is then called primary vorticity. Once created, the secondary vorticity is drawn towards the top of the oval. This movement leads, by Biot-Savart's law, first to a slowing of the descent of the vortices and then to their convergence [24]. The vortices can also transiently move up in this phase. The vortices then accelerate downward because of the implied increase of the induction between the two vortices. Note that the presence of a hot jet can strengthen this dynamics [24]. At the top of the oval, the secondary vorticity convects upward along the symmetry axis of the flow, generally up to flight altitude [25], due to buoyancy and the induction of each half of the secondary vorticity onto the other. There it accumulates and forms a secondary wake which considerably increases the vertical extent of the wake.

The hypothesis, widely supported by several studies [16,17], is that, in the *vortex phase*, the aerodynamic wake of a cruising aircraft is composed of the two tip vortices separated by a distance equal to $\pi/4$ the wing span, corresponding to an (optimal) elliptical loading. The various physics of the interaction between the jet plume and the wake can then simply be approached by playing with the ratio of the jet position to the wing span. It is interesting to see the existing configurations of jet position in today's aircraft. There are actually three variants: at the center plane of the aircraft or along the fuselage (McDonnell-Douglas MD-11 (DC-10), Lockheed L-1011-1 Tristar, Boeing B717 (MD-87), Bombardier CRJ-200, Bombardier CRJ-900, Embraer EMB-140) and at the first third of the wing for twin-engine aircraft (Airbus A320, Boeing B777). For four-engine aircraft, the first jet also lies at about one-third of the span and the second at about two-thirds (Boeing B747, Airbus A380). Our analysis explores only the situation of twin-engine aircraft and lateral positions in the full range between the middle of the aircraft (at the fuselage) and the wing tip. This theoretical approach does not in essence consider the practicality of this variety of position. Yet it is important to question this. Current aircraft, as listed above, feature selected discrete positions from 0 to approximately 70%–75%. More outboard positions hence look quite unconventional. However, the location of the engines is a constrained problem, and the issue of climate impact could change the current practice, if required. Roughly the jet position must first be compatible with the other parts of the aircraft (flaps, ailerons, landing gears, fuselage) and must also be acceptable from a structural point of view. It is from this latter perspective that the outermost positions could be questioned. In this respect one important constraint is also aircraft controllability. In case of engine failure, it could be jeopardized by an engine too far outboard. However, an outboard position can also have advantages, regarding, for instance, the noise radiated to the cabin, ground clearance, and wing bending. Interestingly the Boeing-Bell V-22 Osprey has turboprop engines exactly at the wing tips, indicating feasible in certain cases. Thus while the continuous range of position is hard to fully justify from a practical point of view, it does not seem totally infeasible either, and it clearly presents a strong interest from the fundamental point of view.

To get a simple understanding of the influence of the jet position, it helps to consider the two extreme cases: first, when the jets are fully entrained in the vortex wake and, second, when they are not entrained at all. In the former case, the jets are moved vertically and thus evolve in an external environment made of variable thermodynamic conditions, most notably the ambient temperature changes which affect condensation. If the ice plume is entrained to a lower altitude, one expects ice sublimation because of the higher temperature. This would be beneficial from the radiative impact point of view. In the other case, the jets remain at flight altitude, and external conditions are stable and as cold as they could be. This configuration, which agrees then with the Schmidt-Appleman criterion, appears worst. Some sensitivity studies [13,26] already report on such an influence of the initial jet distribution on the plume evolution, especially for extreme values. The sensitivity of the

jet entrainment process has also been described experimentally by [10] within a few wing spans downstream of an idealized aircraft configuration. The contrail to cirrus transition that may occur at the end of this interaction process has also been shown to depends on many parameters, including the aircraft type. The importance of the near wake is also appraised by the good correlation between the optical impact of contrail of the cirrus phase with regard to the earlier phases [27].

In the light of the important effects of the vortex entrainment and buoyancy on the contrails evolution, the goal of this study is (1) to describe the influence of the position of the jet on the wake dynamics during the vortex phase in a stratified atmosphere and (2) to evaluate the various scenario of optical impact of the early contrails. A parametric approach using simulation is employed to map the entire range of applicable stable stratification and possible jet positions from fuselage to wing tip.

The outline of the paper is the following: Section II describes the model of the flow and ice, Sec. III analyses the influence of the jet positioning and stratification on the flow and the plume evolutions, and Sec. IV describes the optical features of the ice plume and concludes with their dependence on the two parameters.

II. MODEL

A. Flow

The model consists of a 2D pair of counter-rotating vortices and two-engine exhaust plumes that evolve in a stratified atmosphere. This represents a cross section of the aircraft wake during the vortex phase. Recall that this occurs when the ratio R_3 as defined in [4] becomes small, which means that the distance behind the aircraft is sufficient for the whole dynamics of the jet to be negligible compared to the transverse velocity field induced by the vortices. This ratio compares the axial momentum of the jet to the induction effect by the tip vortices and is given by

$$R_3(x) = \frac{\Delta\mathcal{P}}{\rho_0 V_\theta^2 A_{\rm en}(x)} = 16\,\pi\,\frac{\Delta\mathcal{P}}{\rho_0\,\Gamma_0^2}\left(\frac{r(x)}{D(x)}\right)^2. \tag{3}$$

Here $A_{\rm en}(x) = \pi\,D(x)^2/4$ is the cross-sectional area of the jet at a distance x downstream of the engine outlet, $D(x)$ the jet flow section diameter, and $\Delta\mathcal{P}$ the nominal thrust intensity of the engine. As already introduced, Γ_0 is the vortex circulation and ρ_0 the density of air. The jet is located at a distance $r(x)$ from the center of the vortex, far enough to consider that the flow due to the vortex is a potential flow, i.e.,$V_\theta(r) = \Gamma_0/2\pi r$. A semiempirical law for the increment in size of the jet cross section is given by $D(x) = a_D\,x$, with [28]

$$a_D = 0.14\,\frac{\left(1-\frac{U_0}{U_{\rm en}}\right)\left[1+\left(\frac{\rho_0}{\rho_{\rm en}}\right)^{\frac{1}{2}}\right]}{1+\frac{U_0}{U_{\rm en}}\left(\frac{\rho_0}{\rho_{\rm en}}\right)^{\frac{1}{2}}}, \tag{4}$$

where $U_{\rm en}$ and $\rho_{\rm en}$ are the engine jet velocity and density, respectively, and U_0 the aircraft velocity. This formula neglects the compressibility effects, as is done by [4]. This is possible as the jet is adapted (the pressure of the engine exhaust at exit is the same as the atmospheric pressure). The engine produces a nominal thrust intensity

$$\mathcal{P} = \rho_{\rm en}\,U_{\rm en}^2\,A_{\rm en}(x_{\rm out}), \tag{5}$$

where the jet engine exit position is denoted $x_{\rm out}$. For cruising flight, thrust equals drag. The increment of momentum flow induced by the engine with upstream flow U_0 is therefore

$$\Delta\mathcal{P} = \rho_{\rm en}\,U_{\rm en}(U_{\rm en}-U_0)A_{\rm en}(x_{\rm out}). \tag{6}$$

The distances behind the aircraft at which different values of R_3 are reached are shown in Table II, for two different jet spacings. The parameters used for the aircraft are compatible with an A330 and

TABLE II. Distance (scaled by the wingspan b) behind the aircraft at which different values of R_3 are reached. Two cases of jet position are considered.

R_3	10	5	1	0.5	0.1
Engine at 1/3 of the wingspan	2.1	3.0	6.6	9.3	20.9
Engine at 2/3 of the wingspan	0.57	0.81	1.8	2.6	5.8

given in Table I. Note that since the jet is matched ($p_{\text{en}} = p_0$), the ratio of densities is the inverse of that of temperatures: $\rho_0 T_0 = \rho_{\text{en}} T_{\text{en}}$.

During the vortex phase, the atmosphere and the wake interact via buoyancy effects that oppose the downward momentum of the vortices and modify the temperature distribution. Buoyant forces result from the vertical nonuniformity of a quantity called potential temperature,

$$\Theta = T\left(\frac{p_0}{p}\right)^{R/c_p}, \tag{7}$$

which corrects the thermodynamic temperature for adiabatic evolution. The atmosphere is stratified when $\mathrm{d}\Theta/\mathrm{d}z \neq 0$. In this relation, R is the perfect gas constant of dry air and c_p its heat capacity at constant pressure. The Brunt-Väisälä frequency

$$N = \sqrt{\frac{g}{\Theta}\frac{\mathrm{d}\Theta}{\mathrm{d}z}} \tag{8}$$

gives the frequency of the vertical oscillations of air particles when they are disturbed in such an environment (g is the standard gravity). The wake imposes the characteristic time of the wake τ_0 defined in Eq. (2) as the reference timescale and the initial vortex separation b_0 as the reference distance. In this scaled framework, stratification is effectively measured by the inverse Froude number

$$\mathrm{Fr}^{-1} = N\tau_0. \tag{9}$$

For a single aircraft, τ_0 can vary by almost a factor two as a consequence of the weight decrease during flight time. The time τ_0 is also a function of the wingspan. The natural Brunt-Väisälä frequency of the atmosphere at flight altitude lies generally between 0.01 and $0.03\,\mathrm{s}^{-1}$. As a consequence, the possible values for Fr^{-1} range from 0 to 2. The Froude number is set to be uniform in the present setup. In reality, it varies temporally and spatially but with sufficiently slow and large scales so that a constant approximation is locally adequate. Table III displays wake and stratification data for a selection of aircraft.

In a linearly stratified medium, the Navier-Stokes equations simplify into the Boussinesq approximation, in which the flow is considered as a superposition of a fixed atmospheric state and a perturbation state, which here refers to the wake flow. Density variations in this situation result purely from thermal effects. The key of the Boussinesq approximation for wake dynamics relates to the order of magnitude of two dimensionless numbers that are estimated by taking the values from Table III. First, the characteristic length of the problem b_0 is small compared to the characteristic length of the field of potential temperature Θ: $\mathcal{F}^2 \ll \mathrm{Fr}^2$ where a secondary Froude number $\mathcal{F}$ (with no relevance with the dynamics) is defined as

$$\mathcal{F}^2 := \frac{W_0^2}{g b_0} \in [0.1, 1] \times 10^{-2}. \tag{10}$$

Second, the compressible effects are weak compared to the dynamics of the wake: $\mathrm{M}^2 \ll \mathcal{F}^2$ where the Mach number M is defined by

$$\mathrm{M}^2 = \frac{W_0^2}{\gamma R T_0} = W_0^2 \frac{\rho_0}{\gamma p_0} \in [0.8, 5] \times 10^{-5}. \tag{11}$$

TABLE III. Vortex wake and stratification parameters for a common aircraft. The range of Fr^{-1} is for N between $0.01\,\mathrm{s}^{-1}$ to $0.03\,\mathrm{s}^{-1}$. b: wingspan, b_0: vortex separation, Γ_0: vortex circulation, W_0: vortex descend speed, τ_0: vortex timescale, b_{jet}: jet separation.

	CRJ-200	A320	B737	B787	A330	B777	B747		A380	
b (m)	21.2	35.8	35.8	60.1	64.0	64.8	68.4		79.7	
b_0 (m)	16.7	28.1	28.1	47.2	50.3	50.9	53.7		62.6	
$\Gamma_{0,\mathrm{min}}$ ($\mathrm{m}^2\,\mathrm{s}^{-1}$)	93.3	161	161	244	266	326	387		430	
$\Gamma_{0,\mathrm{max}}$ ($\mathrm{m}^2\,\mathrm{s}^{-1}$)	162	296	298	472	506	683	811		893	
$W_{0,\mathrm{min}}$ (ms^{-1})	0.89	0.91	0.91	0.82	0.84	1.02	1.15		1.09	
$W_{0,\mathrm{max}}$ (ms^{-1})	1.55	1.67	1.68	1.59	1.60	2.14	2.40		2.27	
$\tau_{0,\mathrm{min}}$ (s)	10.7	16.8	16.7	29.7	31.4	23.8	22.4		27.6	
$\tau_{0,\mathrm{max}}$ (s)	18.7	30.8	30.9	57.3	59.6	49.9	46.8		57.3	
$\mathrm{Fr}^{-1}_{\mathrm{min}}$	0.107	0.168	0.167	0.297	0.313	0.238	0.224		0.276	
$\mathrm{Fr}^{-1}_{\mathrm{max}}$	0.560	0.923	0.927	1.72	1.79	1.50	1.40		1.72	
b_{jet}/b (%)	20	32	28	32	33	31	34[a]	61[b]	40[a]	67[b]

[a]For the inboard engine.
[b]For the outboard engine.

In these relations γ is the ratio of specific heat capacities. It should be noted that the reference velocity in our dimensionless framework is the initial wake descent velocity W_0 defined in Eq. (1) which is on the order of 1 to $2.5\,\mathrm{ms}^{-1}$ (see Table III), and thus much lower than the cruise speed of an aircraft. This is what explains these small values for the Mach number.

The atmospheric component is decomposed into a uniform component (subscript 0) and a component varying with altitude, with a linear approximation of the local hydrostatic equilibrium (subscript 1). Taking Θ as an example, this gives $\Theta = \theta_0 + \theta_1(z) + \theta'(\boldsymbol{x}, t)$ where $\theta' \ll \theta_0 + \theta_1$ is the flow-induced component. Considering that $\mathcal{F}^2$ measures the ratio between the inertia of the system and the gravitational forces and M^2 the importance of the compressible effects, the flow-induced variables are scaled as follows:

$$\theta' = T_0 \mathcal{F}^2 \theta, \tag{12a}$$

$$p' = \gamma p_0 \mathrm{M}^2 p = \rho_0 W_0^2 p, \tag{12b}$$

$$\rho' = \rho_0 \mathcal{F}^2 \rho. \tag{12c}$$

Soot and water vapor concentrations emitted by the engines are integrated into the model by considering a passive scalar and its transport law. We denote c the concentration of this passive scalar. The passive scalar hypothesis is justified as, at flight altitude, specific humidity is on the order 10^{-4} and induces a negligible influence on the dynamics. Here we recall the normalization of the various variables. Lengths are normalized by the initial vortex spacing b_0 and times by τ_0. The dimensionless governing equations then become [29]

$$\boldsymbol{\nabla} \cdot \boldsymbol{u} = 0, \tag{13a}$$

$$\frac{\mathrm{d}\boldsymbol{u}}{\mathrm{d}t} = -\boldsymbol{\nabla} p + \theta \boldsymbol{e}_z + \frac{1}{\mathrm{Re}} \boldsymbol{\nabla}^2 \boldsymbol{u}, \tag{13b}$$

$$\frac{\mathrm{d}\theta}{\mathrm{d}t} = -\frac{1}{\mathrm{Fr}^2} \boldsymbol{u} \cdot \boldsymbol{e}_z + \frac{1}{\mathrm{Pr}\,\mathrm{Re}} \nabla^2 \theta, \tag{13c}$$

$$\frac{\mathrm{d}c}{\mathrm{d}t} = \frac{1}{\mathrm{Sc}\,\mathrm{Re}} \nabla^2 c, \tag{13d}$$

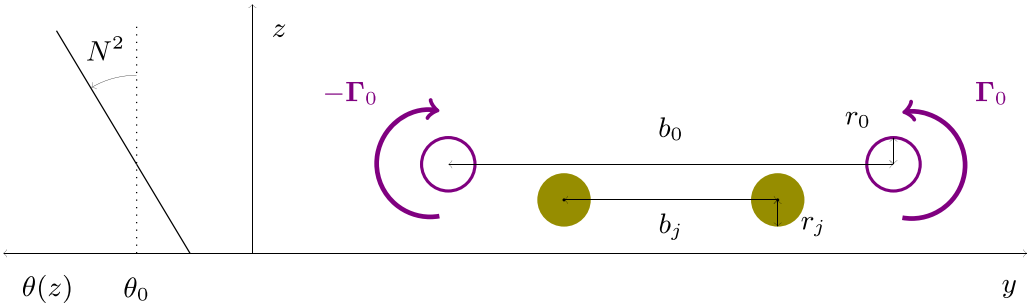

FIG. 1. Setup of the flow taken into consideration for initializing the numerical simulations. The model is symmetric and comprises two Gaussian vortices and two round jets, which support the jet exhaust and potential presence of the contrail ice panache. The schematic shows the atmospheric conditions characterized by the Brunt-Väisälä frequency and the variable jet spacing b_j.

where $\mathrm{Re} = W_0 b_0/\nu$, Pr, and Sc are the Reynolds, Prandtl, and Schmidt numbers of water vapor, respectively, with ν the kinematic viscosity. They are set to $\mathrm{Pr} = 0.7$ [30], $\mathrm{Sc} = 1.3$ [31], and $\mathrm{Re} = 10^4$. The diffusivity κ of soot depends on the diameter d of the particles: $\kappa = d^{-1} \times 10^{-13}$ m^2 s^{-1} [32]. The typical size of particles from jet engines is $d = 10^{-8}$m [33] leading to $\mathrm{Sc}_{\mathrm{soot}} = \nu/\kappa = 4$. However, on account of the high Reynolds number (i.e.,diffusion is negligible compared to advection) and to simplify the setup, we take it equal to that of water vapor: $\mathrm{Sc}_{\mathrm{soot}} = \mathrm{Sc}$.

As discussed earlier, the (turbulent) dynamics of the jet is negligible during the vortex phase. Moreover, trailing vortices have a very low amount of turbulence because the rotational flow is stabilizing according to the Bradshaw-Richardson criterion [34]. Thus, it is the fluid viscosity that dictates the diffusion of the vortices [35]. Furthermore, in the vortex jet interaction in a stratified atmosphere, the dominant dynamical mechanisms are the jet entrainment, stirring by the vortices, and the baroclinic vorticity production, much more than turbulent or viscous diffusion. This justifies the 2D laminar model used in the present study. The flow initialization follows the symmetric scheme presented in Fig. 1. We introduce two Gaussian vortices of radius $r_0 = 0.05\,b$ [36]. The initial distribution of passive scalar and temperature follow a tanh distribution at the location of the jet [11]. The maximum (real) temperature within the jets is fixed at 2 K. Recall that this corresponds to the jet temperature at the beginning of the vortex phase, not that at the exit of the engines. [11] provides simulation data of the jet phase and shows (Fig. 27) that the temperature of the jet at the end of this phase is about $-50\,^\circ$C, which is only little above the ambient. The rapid decrease of the jet temperature, due to its mixing, is also visible in Fig. 4 of [17]. The turbulence of the first stage of the jets is taken into account in the radius r_{jet} of the initial conditions of the passive scalar, i.e.,it is enlarged compared to the engine exit size by the amount caused by turbulent diffusion. We set $r_{\mathrm{jet}} \simeq 0.15\,b$ while the jet exhaust half diameter is $D(x_{\mathrm{out}})/2 \simeq 0.01\,b$. Such an initial condition is commonly used in contrail analysis [11,14,24]. The initial jet lateral position $\bar{b}_{\mathrm{jet}} = b_{\mathrm{jet}}/b$ varies in the range 0 (midplane) to 1 (wing tip). Their vertical position relative to flight level is fixed at $-0.081\,b$ [14]. Keep in mind that scaling here is done in relation to the span b and not the distance between the vortices b_0, to ease the understanding of the jet location along the wing. It is further assumed that stratification has not yet affected the flow at the initial time of the present simulations. A quick calculation allows the estimation of the distance behind the aircraft from which the influence of the buoyant forces becomes significant $x = U_0^2/g$, which corresponds to a hundred aircraft wingspans for a typical cruising speed $U_0 = 250\,\mathrm{ms}^{-1}$. This corresponds to the vortex phase.

Equations (13) are solved using the Nek5000 spectral element code in a 2D setup with polynomials of order 12. The size of the numerical domain is between 100 and 200 elements in y and between 100 and 400 elements in z, depending on the stratification level. The size of the computational domain is between $[-4, 4]$ and $[-6, 6]$ in y, and $[-4, 4]$ and $[-24, 6]$ in z. The large number of

elements is explained by the fine discretization of the mesh that is required at the midplane between the vortices, due to the strong fluid strains that occur at the upper hyperbolic point of the Kelvin oval and the possible close proximity of the vortices. The cost of one simulation is about 100 days of CPU time. The parametric study evaluates 22 b_{jet} values between 0 and 1, and 20 Fr^{-1} values between 0 and 2 amounting to 440 calculations and 120 years of (sequential) CPU time. Using about 3000 processors, the calculations can be done in two weeks.

B. Ice plume

The humidity in the system comes from the natural humidity in the atmosphere, which adds to the humidity released by the aircraft engines. One can then write the decomposition of the partial density of vapor

$$\rho_v = \rho_{v,\text{atm}} + \rho_{v,\text{jet}} \tag{14}$$

as the sum of the contributions of the atmosphere and the jets. The present model follows the approach of [11,14] and makes several assumptions: (1) surface effects (Kelvin effects) are neglected; (2) soot particles act as nuclei for water vapor and there are as many ice particles as there are soot particles; and (3) phase changes are instantaneous and without feedback to the flow and temperature.

In this framework, the condensation of vapor to ice in the jet plume is calculated using an Eulerian description of the distribution of effective radius r_e, mass ρ_i, and density ρ_{soot} of ice crystals. These quantities, whose distribution is not uniform in the domain, are calculated from the passive scalar c and the local thermodynamic properties. The amount of water and soot particle concentration are proportional to c at any time, meaning that there exist α and β such that

$$\rho_{v,\text{jet}} = \alpha\, c, \tag{15a}$$

$$\rho_{\text{soot}} = \beta\, c. \tag{15b}$$

Since $p_v = \rho_v R_v T$ one has

$$p_v = (\rho_{v,\text{atm}} + \rho_{v,\text{jet}}) R_v T =: p_{v,\text{atm}} + p_{v,\text{jet}}, \tag{16}$$

then

$$p_{v,\text{jet}} = \alpha R_v T c. \tag{17}$$

We assume that before the vortex phase (i.e.,during the jet and the deflection phase) the plume has undergone an isobaric dilution between the initial jet and atmospheric conditions such that at initial time $t = 0$ [37]:

$$p_v^{t=0} - p_{v,\text{atm}} = G(T^{t=0} - T_{\text{atm}}), \tag{18}$$

i.e.,

$$p_{v,\text{jet}}^{t=0} = G\, T_{\text{jet}}^{t=0}, \tag{19}$$

where

$$G = \frac{c_p\, p_0\, EI_{\text{H}_2\text{O}}}{\left(M_{\text{H}_2\text{O}}/M_{\text{air}}\right) Q_{\text{fuel}}\,(1-\eta)} \tag{20}$$

is the slope of the straight line of the isobaric evolution of the jet in a p_v-T diagram, with $c_p = 1004\,\text{Jkg}^{-1}\,\text{K}^{-1}$ the specific heat capacity of air, $M_{\text{H}_2\text{O}}/M_{\text{air}} = 0.622$ the ratio of the molar masses of water and air, $EI_{\text{H}_2\text{O}}$ and Q_{fuel} the water emission index and the heat of combustion of the fuel used, respectively, and η the overall propulsive efficiency of the aircraft in cruise. Note that $t = 0$ is the beginning of the vortex phase. Quantities are therefore different from their value immediately after engine exit, since the plume has been much diluted in the atmosphere during the jet phase. The

Boussinesq approximation gives $T^{t=0} = T_0$ at order 1, thus

$$\alpha R_v T_0 c^{t=0} = G T_{\text{jet}}^{t=0}. \tag{21}$$

As a consequence $T_{\text{jet}}^{t=0}$ is proportional to $c^{t=0}$, which we denote $T_{\text{jet}}^{t=0} = T_{\max} c^{t=0}$. Then

$$\alpha = \frac{G T_{\max}}{R_v T_0}. \tag{22}$$

Moreover, the ratio α/β of the total amount of water emitted over the total amount of soot is constant over time with value $EI_{\text{H}_2\text{O}}/EI_{\text{soot}}$, so

$$\beta = \frac{EI_{\text{soot}}}{EI_{\text{H}_2\text{O}}} \frac{G T_{\max}}{R_v T_0}. \tag{23}$$

Hereafter, we consider the values for a kerosene-fueled engine. They are $G = 1.64\,\text{Pa K}^{-1}$, $EI_{\text{soot}} = 2.8 \times 10^{14}\,\text{kg}^{-1}$, and $EI_{\text{H}_2\text{O}} = 1.23\,\text{kgkg}^{-1}$ [37].

Assuming that at equilibrium the vapor pressure is equal to the saturation vapor pressure (i.e.,the mass of ice, when present, is such that the vapor pressure is equal to the saturation vapor pressure), the local density of ice (total mass of ice particles in a volume of air) is derived from the perfect gas equation

$$\rho_i = \frac{p_v - p_{\text{sat},i}}{R_v T} \mathbb{1}_{p_v \geqslant p_{\text{sat},i}} = (\rho_v - \rho_{\text{sat},i}) \mathbb{1}_{\rho_v \geqslant \rho_{\text{sat},i}}, \tag{24}$$

where we denote by analogy $p_{\text{sat},i}(T) = \rho_{\text{sat},i}(T) R_v T$. We denote $\mathbb{1}_A$ the indicator function of the set A. We assume that ice crystals can be represented approximately by randomly oriented hexagonal-based cylinders whose size can be characterized by an effective radius r_e [38], as their expected size is about between 10 and 20 nm [39]. If a is the radius of the base of the hexagon and L the length of the cylinder, the volume and the area of the crystal are, respectively,

$$V = \frac{3\sqrt{3}}{2} a^2 L, \tag{25a}$$

$$A = 6\left(a^2 \frac{\sqrt{3}}{2} + aL\right). \tag{25b}$$

According to [39], the aspect ratio of the crystals depends on their length such that $L/(2a) = L^{0.4}$. Then

$$A = 2\left(\frac{3\sqrt{3}}{8}\right)^{\frac{5}{11}} V^{\frac{6}{11}} + 3\left(\frac{3\sqrt{3}}{8}\right)^{-\frac{8}{11}} V^{\frac{8}{11}}. \tag{26}$$

The local mass of a crystal is the ratio of the total mass of ice particles in a volume of air ρ_i on the number of soot in this volume ρ_{soot}. The volume of a crystal is obtained by dividing the mass of a crystal $\rho_i/\rho_{\text{soot}}$ by the density of ice d_i ($917\,\text{kgm}^{-3}$ at flight altitude):

$$V = \frac{\rho_i}{\rho_{\text{soot}}} \frac{1}{d_i}. \tag{27}$$

The effective radius is then computed taking

$$r_e = \sqrt{\frac{A}{4\pi}}. \tag{28}$$

With the previous formulas, it is possible to comment on hypothesis 3, which consists in neglecting the feedback of the phase change on the temperature of the fluid. Considering, for

instance, that $RH_i = 140\%$, the typical maximum mass density is $\rho_{i,\max} \sim 2 \times 10^{-5}\,\mathrm{kgm}^{-3}$ and the neglected temperature variation is

$$\Delta T_{\mathrm{err}} = -\frac{\rho_i\, L_{\mathrm{sub}}}{c_p\, \rho_0} \leqslant 0.15\,\mathrm{K} \tag{29}$$

with $L_{\mathrm{sub}} = -2837\,\mathrm{kJkg}^{-1}$ the latent heat of sublimation of water at 220 K. Given the typical temperature difference across the domain ∼2 K, the difference due to the assumption is less than 10%. Furthermore it is important to note that there is no account of history in the evolution of the ice content as it is purely driven by the immediate offset to the saturation curve. While being simple, the present physical model offers the main ingredients for the evaluation of the plume evolution and does so at an acceptable computational cost, hence allowing the present parametric study.

III. FLOW EVOLUTION

A. Influence of stratification on the vortex wake

This section is dedicated to the evolution of the vortex flow and effect of the Brunt-Väisälä frequency. Similar simulations were carried out by [23–25,40,41]. One difficulty is to run the simulation over a long time ($t = 8.5\,\tau_0$) when the Froude number is close to 1. Indeed, in these cases the flow has small spatial scales that require a particularly fine mesh. We provide novel results for these conditions. The evolution of the wake altitude for various stratification levels is shown in Fig. 2(a) using the vorticity extrema as the vortex locator. Note that there were no hot jets in these simulations. When there is no stratification, the vortex pair descends at constant velocity W_0 [see Fig. 2(b)], the distance between the vortices varies marginally [see Fig. 2(c)], and their circulation decreases only by diffusion, which is weak. When the stratification is small ($\mathrm{Fr}^{-1} \leqslant 0.9$), the descent of the wake slows down at around $t = 1$ and then accelerates sharply at around $t = 4$. For intermediate levels ($0.9 \leqslant \mathrm{Fr}^{-1} \leqslant 1.2$), the descent of the wake stops at $t = 2$, the wake then rises again somehow, and then it finally descends again at a much higher speed. The comparison between the descent velocity shown in Fig. 2(b), and the distance between the vortices shown in Fig. 2(c) allows one to notice that the increase of the descent speed is synchronous with the increased proximity of the vortices. This can be explained by the fact that the mutual induction of the two vortices is inversely proportional to their separation. Above the threshold value $\mathrm{Fr}^{-1} = 1.2$, the wake stays at flight altitude. When the atmosphere is stratified, the vorticity distribution separates into two parts: the two patches of vorticity associated with the initial vortices (that is called primary vorticity) and the vorticity generated by buoyancy (that is called secondary vorticity), of opposite sign, which is created at the boundary of the Kelvin oval of the primary vortex pair. The Kelvin oval is the envelope of the fluid that rotates around the primary vortices and moves with them in their descent. This can be understood by writing the Helmholtz equation for the axial vorticity

$$\frac{\mathrm{d}\omega}{\mathrm{d}t} = \frac{\partial\theta}{\partial y} + \frac{1}{\mathrm{Re}}\nabla^2\omega. \tag{30}$$

The source term $\frac{\partial\theta}{\partial y}$ in this equation results from the baroclinic term $\frac{1}{\rho^2}\boldsymbol{\nabla}\rho \times \boldsymbol{\nabla}p$ derived from the Boussinesq approximation. The temperature differential at the boundary of the Kelvin oval results from the combined effects of stratification and wake descent. The interplay of these effects creates a horizontal potential temperature gradient, as shown in Fig. 3(a). Secondary vorticity of opposite sign is thus generated at the boundary of the Kelvin oval, as shown in Fig. 3(b). The secondary vorticity does not circulate around the vortices but is diverted upwards and rises along the axis of symmetry (see Fig. 4). This baroclinic vorticity is indeed brought to the top hyperbolic point and there taken upward by the flow that passes by the oval [23,40]. The induction of the baroclinic vorticity upon itself also leads to this upward motion. The creation of secondary vorticity coincides with the inflection of the descent of the primary vortices. Indeed, the action induced by the secondary vorticity on the primary vortices is a vertical velocity directed upwards. Furthermore, as noted by

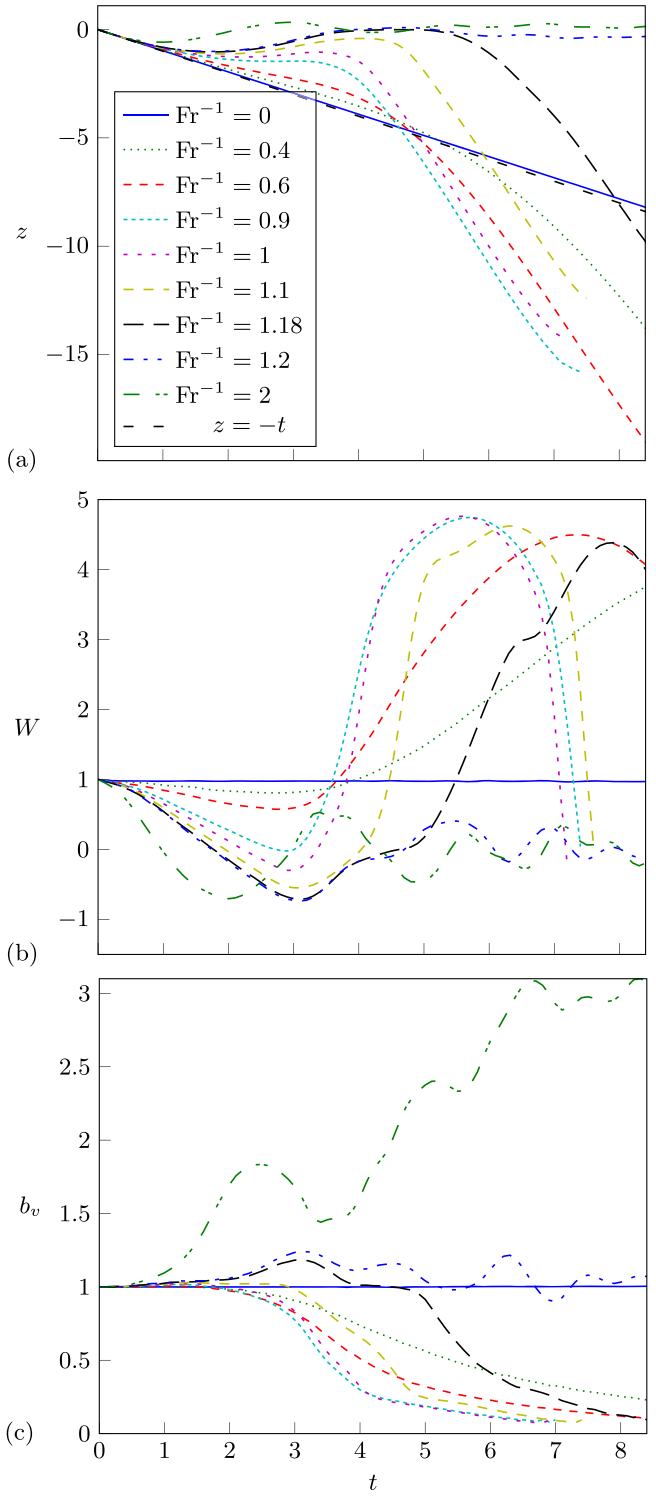

FIG. 2. (a) Altitude of the vortices as a function of time for different values of Fr^{-1}. (b) Descent velocity of the pair of vortices. (c) Distance between the vortices. Distances are normalized by b_0, time by τ_0, and velocity by $W_0 = \Gamma_0/(2\pi\, b_0)$.

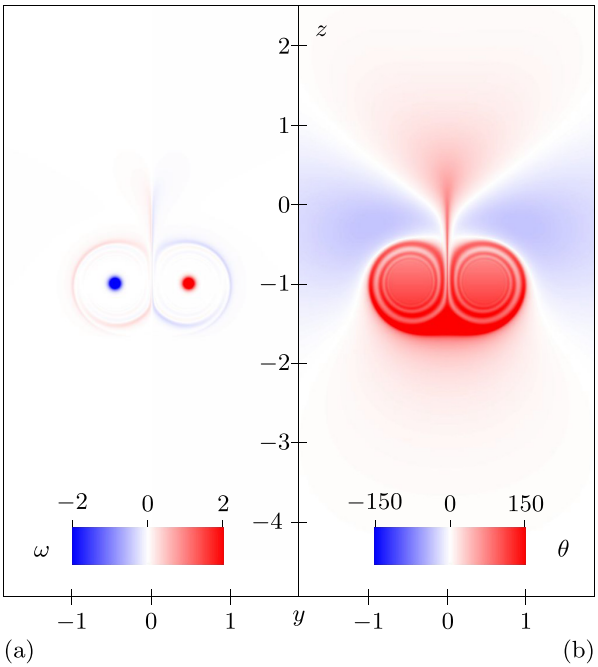

FIG. 3. (a) Vorticity and (b) perturbation of potential temperature fields at $t = 2\,\tau_0$ for $\mathrm{Fr}^{-1} = 1$. All distances are normalized by b_0.

[25], secondary vorticity forms along the streamline that bounds the Kelvin oval and is therefore stronger above the vortices than below, leading to the contraction of the vortex pair. In Fig. 4 one can see that the primary vortices have significantly moved closer together and that the secondary vorticity has escaped from the oval along the axis of symmetry. It then forms a so-called secondary wake at the flight altitude where the width of its horizontal distribution increases.

B. Influence of the hot plume on the vortex wake

Figure 5 compares the altitude of the primary vortices in the absence of a jet and with a jet of maximum temperature difference 2 K (recall that this corresponds to the jet temperature at the beginning of the vortex phase) for the time index $t = 5\,\tau_0$. As expected [24], the presence of a hot jet strengthens the descent of the vortices. As the temperature gradient is larger at the frontier of the Kelvin oval, more baroclinic vorticity is created. This effect depends, however, on the position of the jet. When the jet is at the level of the plane of symmetry of the aircraft ($\bar{b}_{\mathrm{jet}} = 0$), it does not affect the primary vortices. When it is closer to the core of the vortices ($0.4 \leqslant \bar{b}_{\mathrm{jet}} \leqslant 1$), it has two effects. First, when Fr^{-1} is close to 1, the vortices descend lower. Moreover, the threshold between the intermediate (slight rise of the vortices and then faster descent) and high (no descent of the vortices) values of stratification is at higher Fr^{-1}. Between the two regimes ($0 \leqslant \bar{b}_{\mathrm{jet}} \leqslant 0.4$), the altitude to which the wake descends increases with $\bar{b}_{\mathrm{jet}}$ as does the threshold between the intermediate and high values of Fr^{-1}. One can notice that the value of the threshold admits a maximum around $\bar{b}_{\mathrm{jet}} = 0.33$ before decreasing slightly.

C. Comparison with previous studies

A comparison of the vortex trajectory with previous studies [24,25,41] is shown in Fig. 6. The calculation of Spalart [25] takes as initial condition an elliptical vorticity sheet, which forms the two

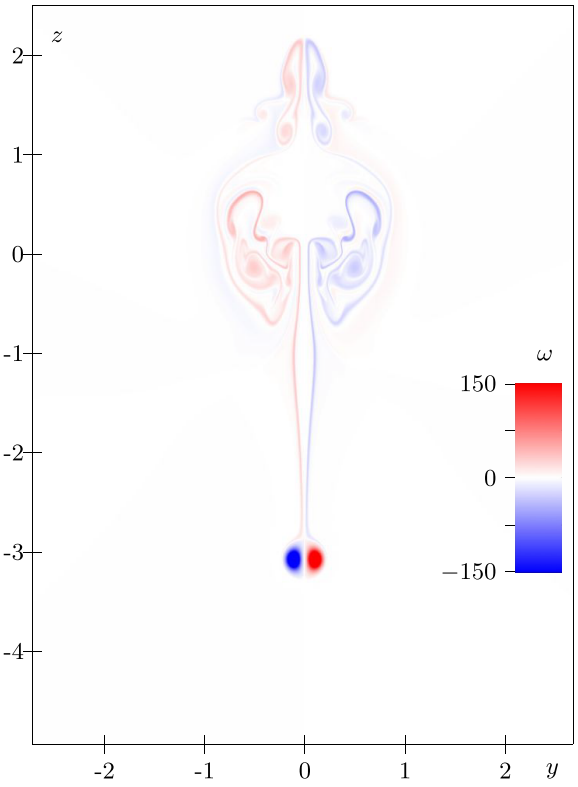

FIG. 4. Vorticity field at $t = 4.5\ \tau_0$ for $\mathrm{Fr}^{-1} = 1$. All distances are normalized by b_0.

vortices after roll-up. We therefore also show the trajectory of our vortices with this initialization to facilitate the comparison. Spalart [25] notes that stratification brings the vortices closer together, leading to an increase in the descent velocity. He also notes that the circulation of the vortices is preserved, and the occurrence of a rebound when stratification is sufficiently high. He further makes the observation of the build-up of baroclinic vorticity and of the consequent formation of the secondary wake. The present vortex trajectories match well his, as does the observed dynamics with his conclusions.

Garten *et al.* [41] looks at the production of baroclinic vorticity and shows that it is responsible for the vortices moving towards or away from each other, depending on the value of the Froude number. The vortex trajectories coincide well with ours.

As analyzed in Sec. III B, the hot jets have a slight influence on the dynamics of the vortices. This effect was already observed by [24]. The agreement on the trajectories is not very good in terms of altitude; however, we suggest that this is due to the difference in the initial temperature field (which is 10 K in his work).

D. Jet exhaust evolution

The evolution of the engine plume is governed by the initial rolling around the primary vortices. Figure 7 shows the time sequence of the field of passive scalar c, which models the plume, for several values of Fr^{-1} and $\bar{b}_{\mathrm{jet}}$, and Fig. 8 for several values of the Froude number for the position $\bar{b}_{\mathrm{jet}} = 0.335$ corresponding to a twin-engine aircraft. The spiral of the winding can be seen in the first column of these figures. Stratification has no effect at this stage since the descent is low [see Fig. 2(a)]. The plume then forms a ring around each vortex (see second column). As long as the

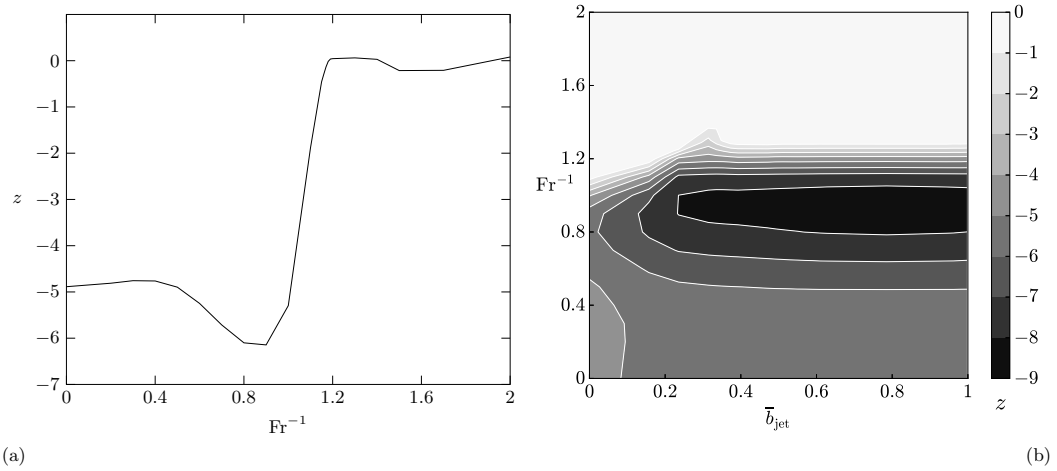

FIG. 5. (a) Altitude of the vortex dipole at $t = 5\,\tau_0$ when there is no jet. (b) Altitude of the vortex dipole at $t = 5\,\tau_0$, when there is a jet, as a function of Fr^{-1} and $\bar{b}_{\rm jet}$.

Kelvin wake is sufficiently large to contain the plume, the latter descends along with the vortices. This is the case for weak stratification levels (see first row) or when the plume is initially very close to the vortices (Fig. 7, last row, until $t = 2.5\,\tau_0$). For intermediate levels, most or all of the jet plume escapes from the oval, becomes diverted across the top of the oval boundary, and is then driven upwards with the secondary vorticity. This brings part of the plume back to flight altitude (see the middle row for $t = 3.5\,\tau_0$ of Fig. 7, and the middle row for $t = 3.5\,\tau_0$ of Fig. 8). These two rows compare favorably with Fig. 5 in [24]. For high levels of stratification, the vortex pair does not descend and the plume maintains its ring shape around the vortices (see the last row of Fig. 8). The oval thus separates two regions of the plane where the flow, and therefore the plume, behave very differently. Everything inside descends with the main vortices, while everything outside extends vertically and rises towards flight altitude with the secondary wake. This behavior depends on stratification and initial jet position, which can be assessed using the mean plume altitude, defined as the average of the altitudes weighted by the amount of passive scalar. The result is shown in Fig. 9(a). Three distinct regions can be identified. When $\mathrm{Fr}^{-1} \geqslant 1.3$ the plume is always located at flight altitude. When $\mathrm{Fr}^{-1} \leqslant 0.5$ and $\bar{b}_{\rm jet} \geqslant 0.4$ the plume descends by a distance that mostly depends on the Froude number. The lowest altitude is reached for $\mathrm{Fr}^{-1} = 0.7$ and $\bar{b}_{\rm jet} = 0.8$. In the intermediate regime, there is a critical threshold

$$\mathrm{Fr}^{-1} \simeq \alpha(\bar{t} - 5)\,\bar{b}_{\rm jet} + \beta(\bar{t} - 5), \tag{31}$$

with $\alpha(\bar{t}) = 0.75 - 0.07\,\bar{t}$ and $\beta(\bar{t}) = 0.25 - 0.07\,\bar{t}$, above which the plume exceeds flight altitude and below which it descends by a distance that depends on both parameters. This threshold corresponds to the case when the barycentre of plume is above the vortices from a distance greater than $2\,b_0$, in the $\bar{b}_{\rm jet} \in [0.1, 0.8]$ zone. It draws the frontier between cases when the plume stays in the Kelvin oval and the cases when it is entrained in the secondary wake. As for the thermodynamic evolution of the plume, we shall see later that the existence of such a marked threshold is very remarkable and means that important phenomena occur within a narrow range of parameter space. The level lines are very tightly packed along this line, which separates two very distinct regions of the map in terms of plume altitude. This has a direct influence on ice mass, and therefore on optical impact. Figure 9(b) shows these regimes using the difference between the average altitude of the plume and the altitude of the primary wake. In the first and second cases, the plume and the vortices are at the same altitude. In the intermediate regime, all or part of the plume is driven by the secondary vorticity away from the main wake. In summary stratification and jet to vortex

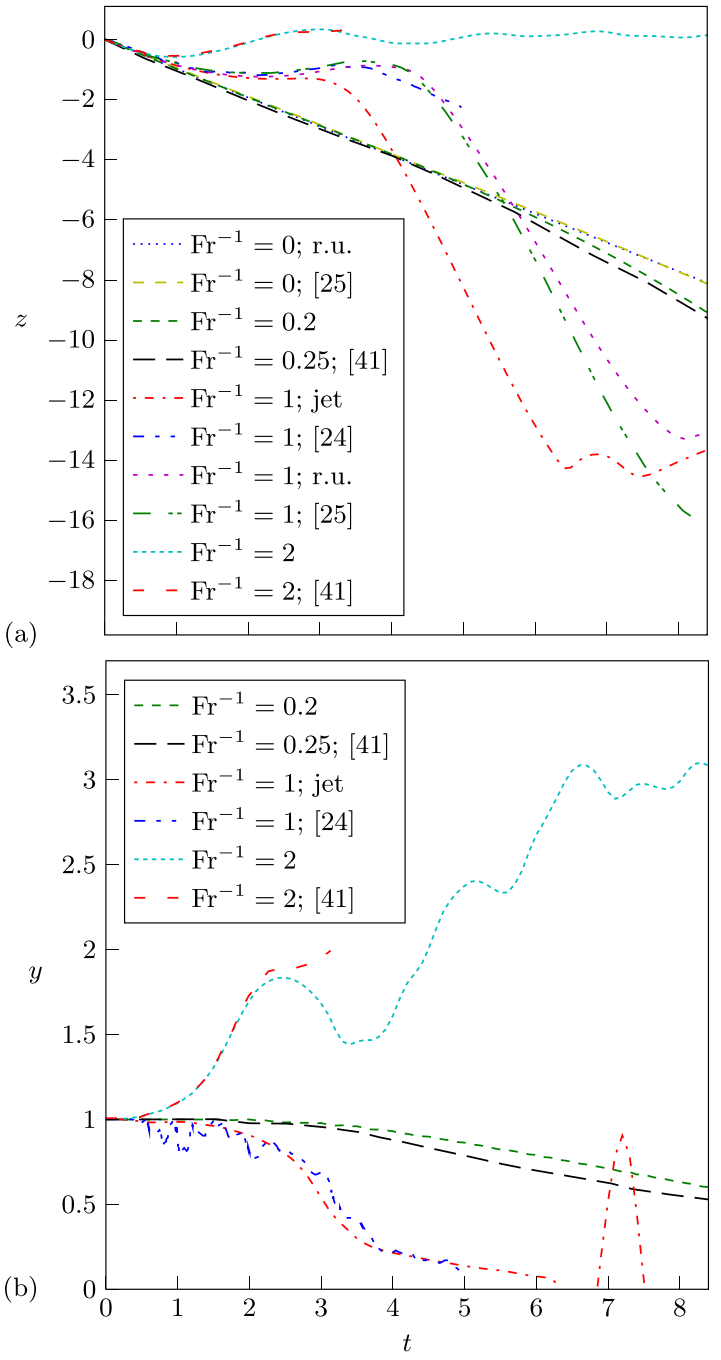

FIG. 6. Comparison of vortex trajectories with other studies: (a) altitude and (b) spacing. "r.u.": the initialization is a vorticity sheet that rolls up in the first moments of the simulation. "jet": the simulation is initialized with the two jets such that $\bar{b}_{\text{jet}} = 0.335$.

distance are determining factors on the evolution of the altitude and the distribution of the plume. The outcome of the optical properties of the ice plume is explored in the final section.

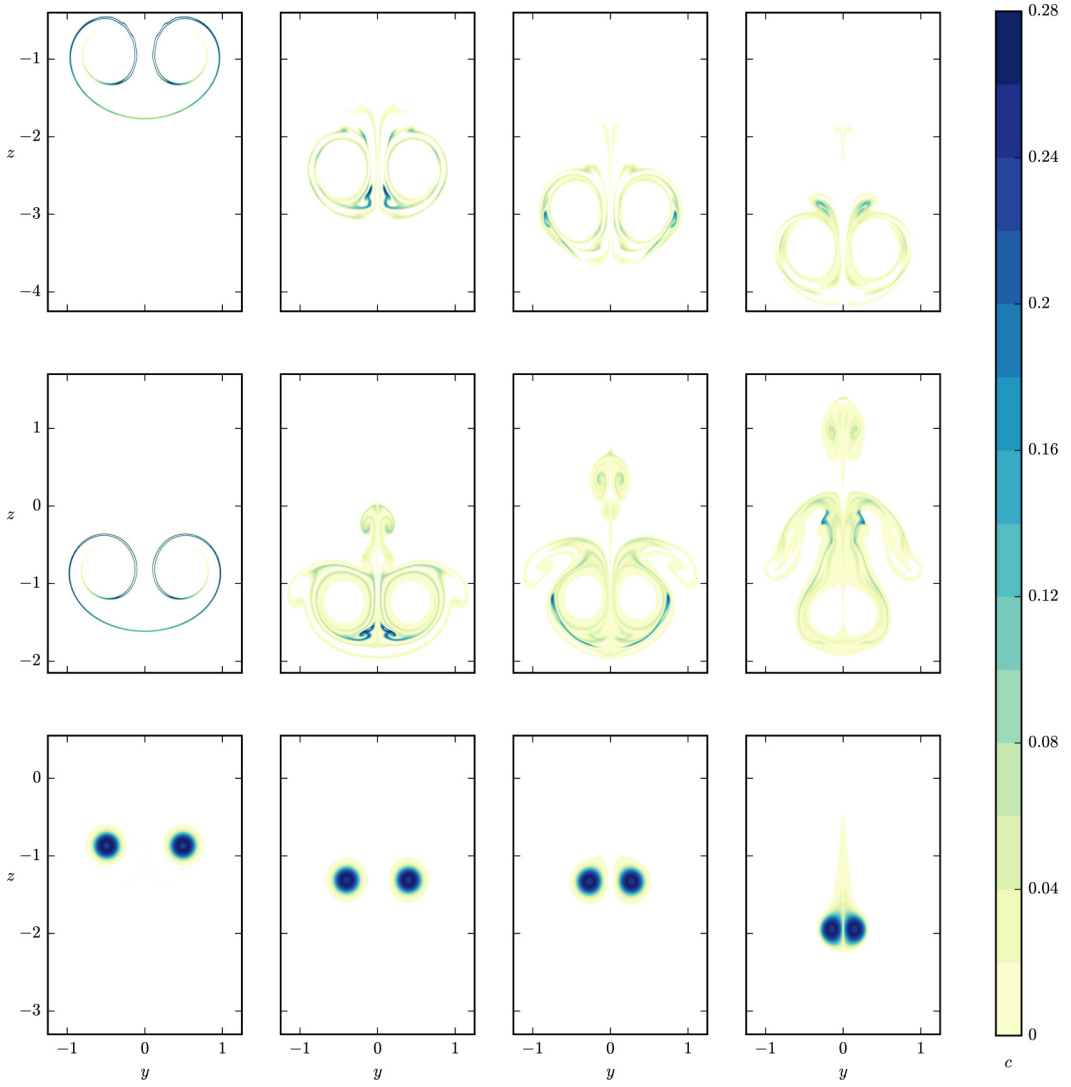

FIG. 7. Evolution of the passive scalar field over time. From top to bottom: $\mathrm{Fr}^{-1} = 0.2$, $\bar{b}_{\mathrm{jet}} = 0.16$; $\mathrm{Fr}^{-1} = 1$, $\bar{b}_{\mathrm{jet}} = 0.16$; $\mathrm{Fr}^{-1} = 1$, $\bar{b}_{\mathrm{jet}} = 0.79$. From left to right: $t = \tau_0$, 2.5 τ_0, 3 τ_0, 3.5 τ_0.

We have placed in Fig. 9(b) the possible parameter ranges for different twin-engine aircraft. These segments correspond to the maximum and minimum mass of the selected aircraft, using a usual interval of Brunt-Väisälä frequencies: from 0.01 to 0.03 s^{-1}. We notice that most of them cross the aforementioned boundary between the intermediate and high levels of stratification and are mostly in the upper part. It is then understood that the plume is no longer located in the vortices at the end of the vortex phase in many cases. Since the observation of early contrails is the only way to see the flow visually from the ground, this explains for instance why it is not systematic to observe Crow instability that affects the primary vortices behind airliners.

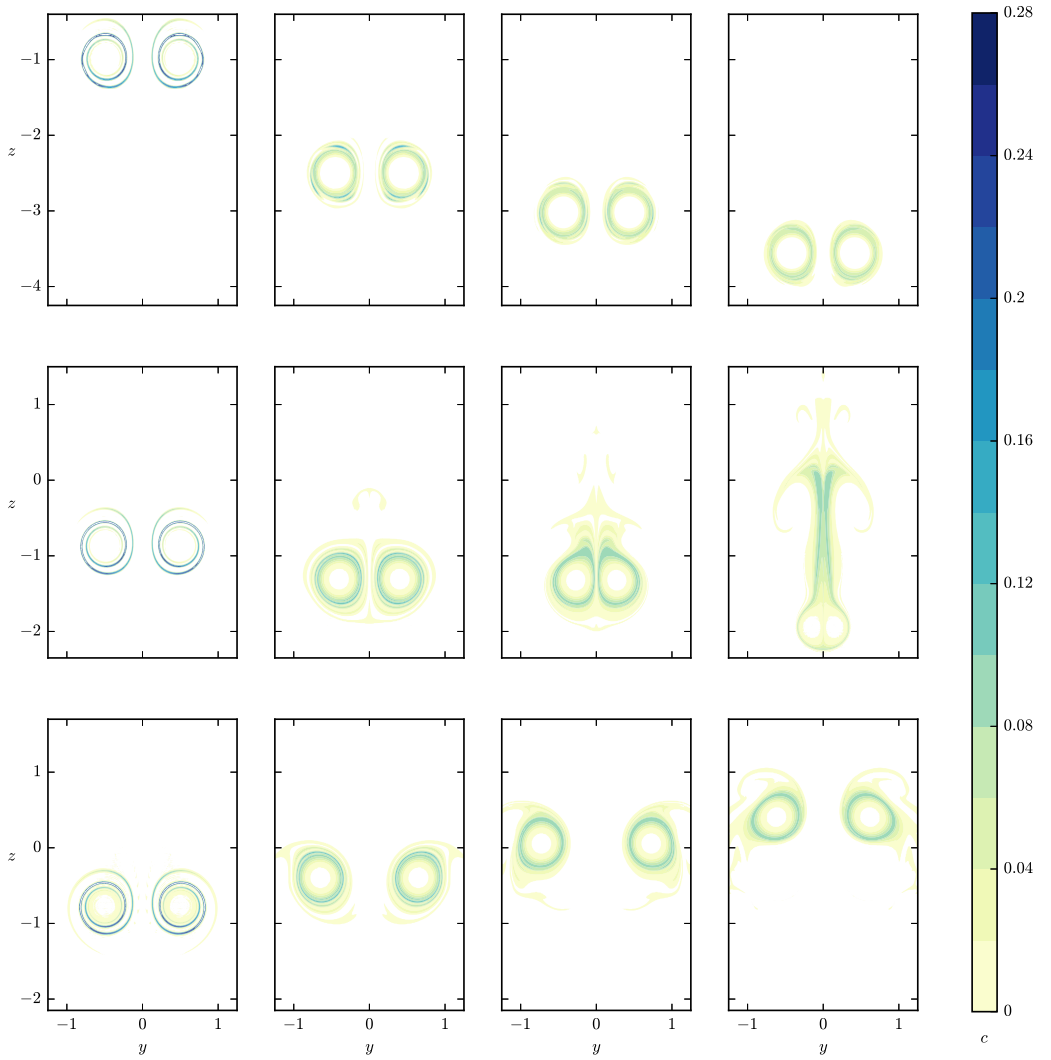

FIG. 8. Evolution of the passive scalar field over time for $\bar{b}_{\text{jet}} = 0.335$. From top to bottom: $\text{Fr}^{-1} = 0.2$, $\text{Fr}^{-1} = 1$, $\text{Fr}^{-1} = 1.4$. From left to right: $t = \tau_0$, 2.5 τ_0, 3 τ_0, 3.5 τ_0.

E. Comparison between the 2D and 3D dynamics

The 2D constraint of the present simulations precludes the capture of the real turbulent dynamics of the secondary wake. Instead, the secondary wake sustains an inverse cascade that favors the formation of larger vortices in the last stages of the flow evolution displayed in the results. The purpose of this section is to make clear that the dynamics of the secondary wake is sufficiently realistic. The small structures induced by the rising secondary wake and baroclinic torque in reality should induce smaller scale 3D movements. Only fully 3D simulation can capture these effects. While this is a limitation to the present simulation, the objective of the 2D approach, that is, to predict the vertical dispersion of the wake, is well achieved.

A 3D computation, much more expensive, is performed for the purpose of comparison, for $\text{Fr}^{-1} = 1$ and $\bar{b}_{\text{jet}} = 0.335$. The bounds in the transverse plane are the same as in the 2D study, as are the boundary conditions. In the direction of flight, the domain is one wing span long and the

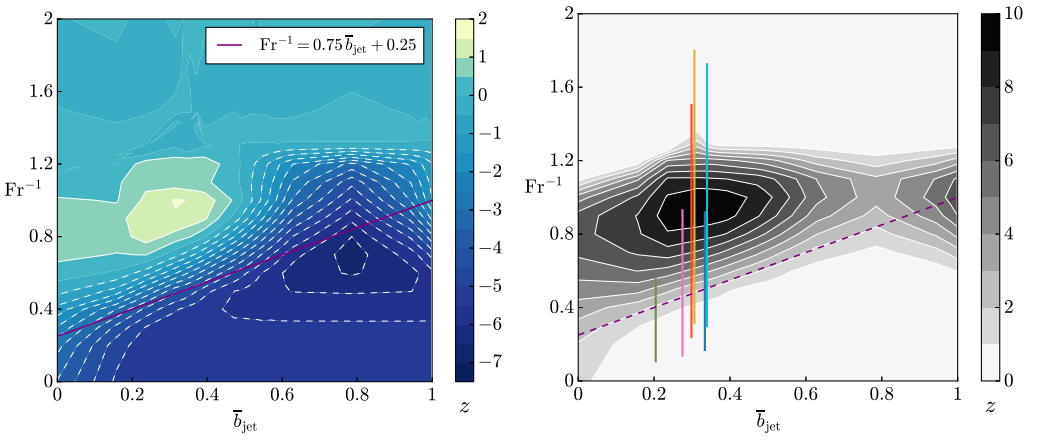

FIG. 9. (a) Mean altitude of the plume and (b) difference between the mean altitude of the plume and that of the vortices at $t = 5\,\tau_0$ as a function of Fr^{-1} and $\bar{b}_{\mathrm{jet}}$. The purple dashed line is the same in both panels. It corresponds to the threshold in the parameters where the plume is on average two characteristic lengths above the vortices, in the $b_{\mathrm{jet}} \in [0.1, 0.8]$ zone. The vertical lines represent the range of possible parameters for a selection of twin-engine aircraft (from left to right): CRJ, B737, B777, A330, A320, B787.

boundary conditions are periodic. The evolution of the altitude of the vortices and plumes is shown in Fig. 10. The value of Froude number is chosen such that a significant secondary wake forms and develops. The value of the initial spacing between the jet plumes is representative of most current long- and medium-range twin-engine aircraft and allows the plumes to be entrained in the secondary wake. The 2D and 3D simulations give very similar results in terms of vortex and plume trajectories.

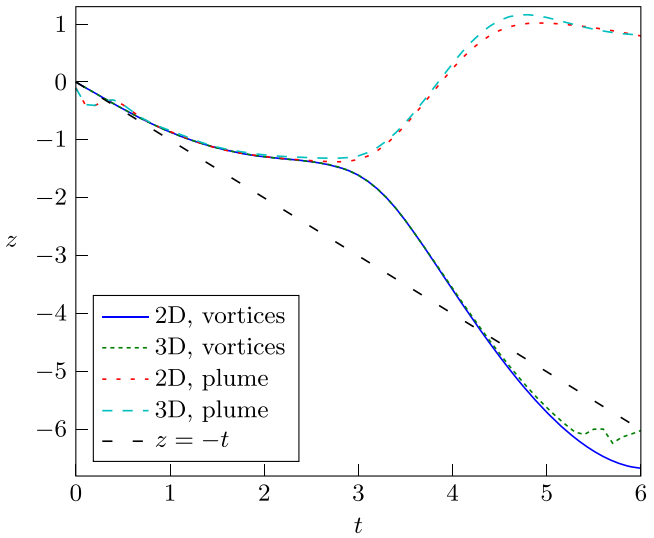

FIG. 10. Comparison between primary vortices and passive scalar altitude evolution for 2D and 3D dynamics at $\mathrm{Re} = 10^3$, $\mathrm{Fr}^{-1} = 1$, and $\bar{b}_{\mathrm{jet}} = 0.335$.

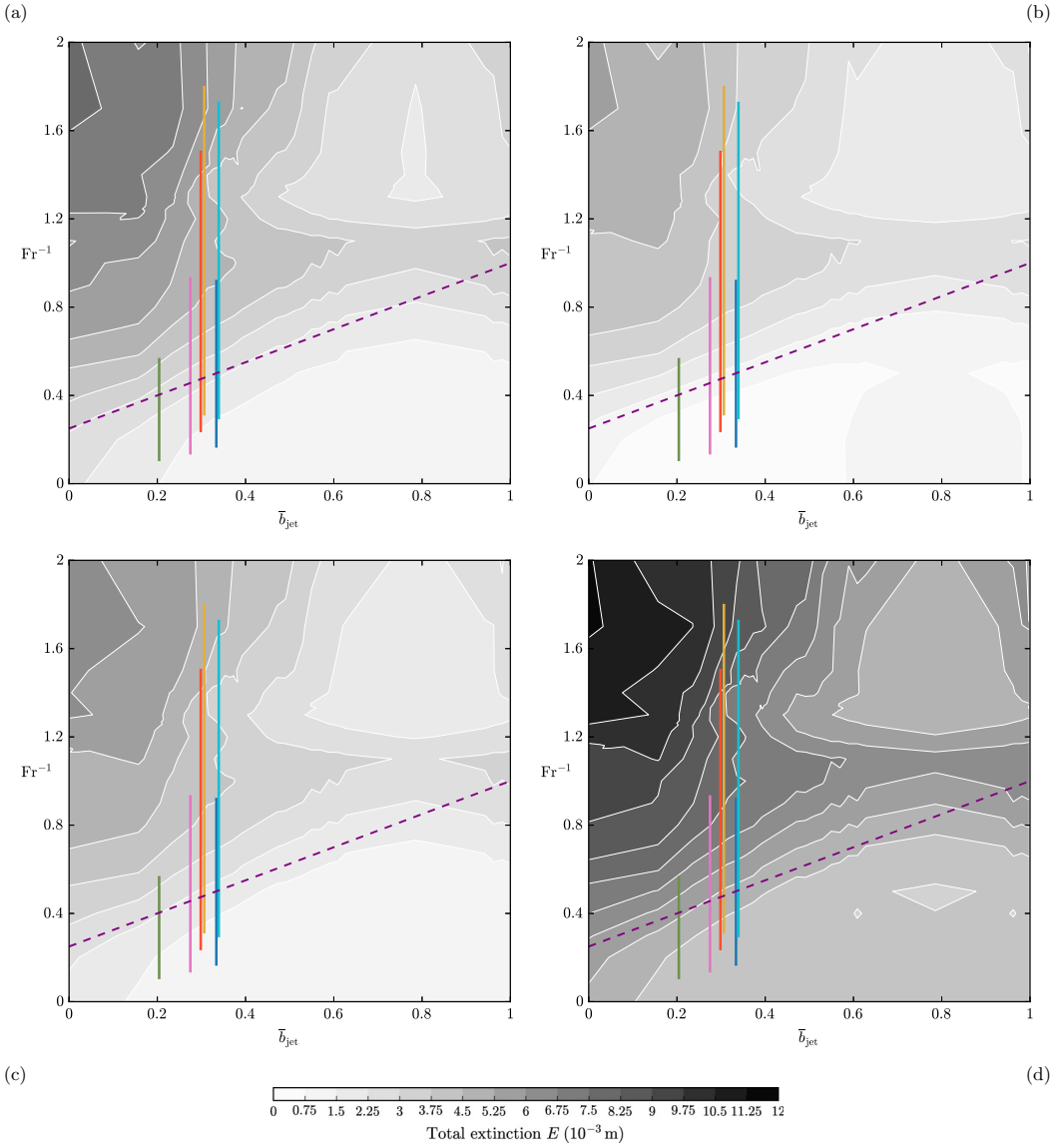

FIG. 11. Total extinction E for (a) $RH = 140\%$ and (b) $RH = 120\%$ at $t = 5\,\tau_0$. In (c) only half of the soot are nuclei and (d) considers the emission index of water for a liquid hydrogen engine for $RH = 140\%$. The vertical lines represent the range of possible parameters for a selection of twin-engine aircraft (from left to right): CRJ, B737, B777, A330, A320, B787. For the purple dashed line legend, see Fig. 9.

IV. OPTICAL PROPERTIES

A. Optical thickness and total extinction

Calculations of the distributions of ice mass per volume ρ_i and crystal effective radius r_e provide an estimate of the energy absorbed by an ice cloud and thus of its potential effect on the radiative balance. For this we are interested in the relative variation in intensity across the entire transverse

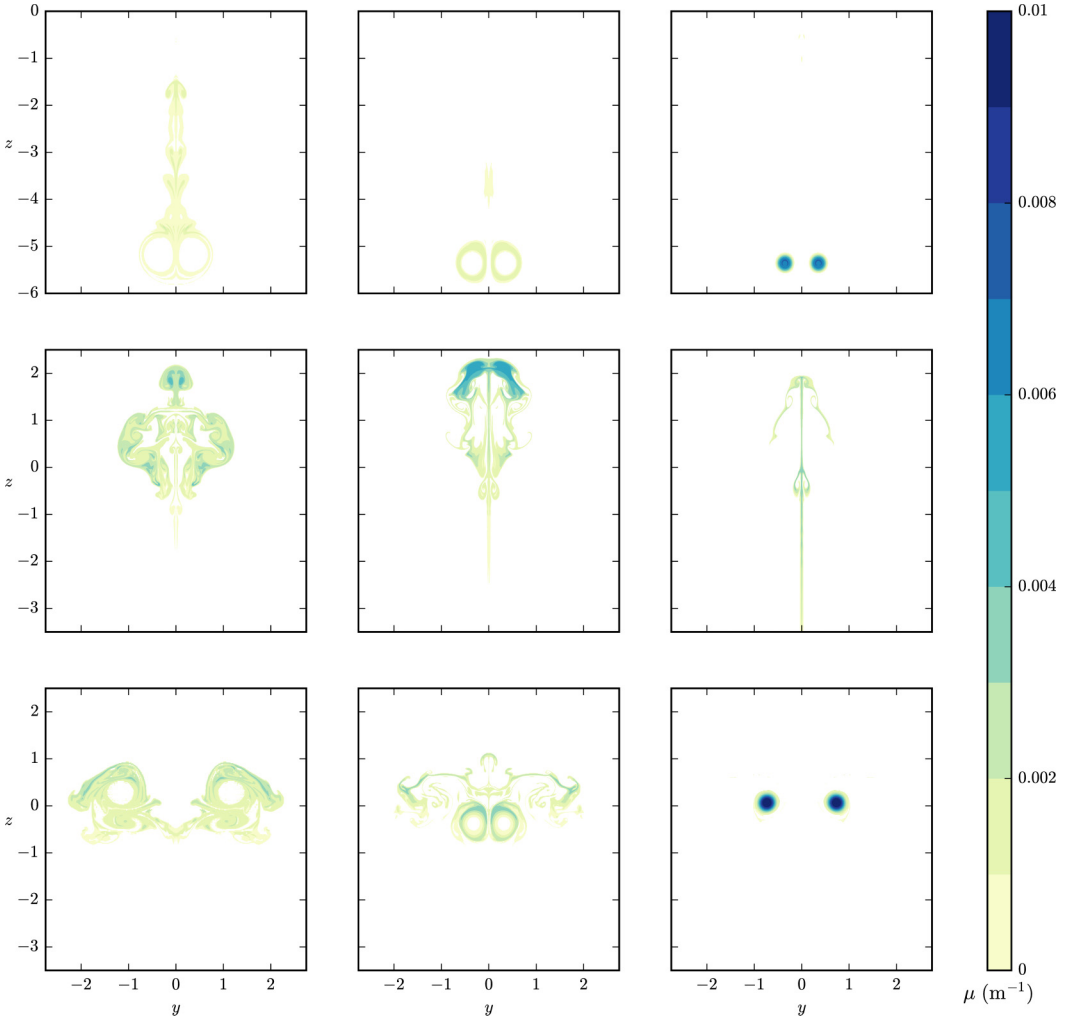

FIG. 12. Attenuation coefficient μ at $t = 5\,\tau_0$ for $RH_i = 130\%$. From left to right $\bar{b}_{\text{jet}} = 0.16$, 0.31, and 0.79. From top to bottom $\text{Fr}^{-1} = 0.2$, 1, and 1.4.

extent of the cloud, called total extinction and defined by

$$E = \int \frac{\mathcal{I}_0 - \mathcal{I}}{\mathcal{I}_0}\,\mathrm{d}y. \tag{32}$$

In this relation, $\mathcal{I}$ and $\mathcal{I}_0$ are the transmitted and incident intensities of a vertical ray of light passing through the medium, respectively. Their ratio is called transmittance $\mathcal{T} = \mathcal{I}/\mathcal{I}_0$ and can be calculated from the optical thickness $\tau = -\ln \mathcal{T}$, which is the integral over the vertical direction of the attenuation coefficient μ:

$$\tau = \int \mu(z)\,\mathrm{d}z. \tag{33}$$

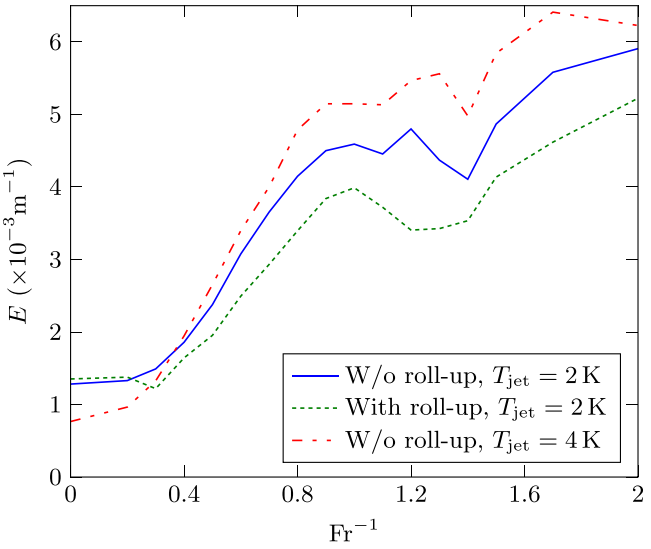

FIG. 13. Comparison of extinction value without and with a roll-up, and with a doubled initial jet temperature for a typical jet position of a twin-engine aircraft ($\bar{b}_{\mathrm{jet}} = 0.335$).

The attenuation coefficient is obtained from the crystal effective radius and ice mass distributions by the formula

$$\mu = \rho_i \left(a + \frac{b}{r_e} \right), \tag{34}$$

where $a = 3.448\ \mathrm{m^2\,kg^{-1}}$ and $b = 2.431 \times 10^{-3}\ \mathrm{m^3\,kg^{-1}}$. The values of a and b are independent upon wavelength for wavelengths between 250 and 3500 nm [38]. The effective crystal radius is of the order of 10^{-6} to 10^{-5} m. Thus, the dominant term in the calculation of the attenuation coefficient is $\rho_i b / r_e$. The total extinction yields

$$\begin{aligned} E &= \int 1 - \mathrm{e}^{-\tau(y)} \mathrm{d}y = \int 1 - \exp\left[- \int \mu(y,z)\,\mathrm{d}z \right] \mathrm{d}y \\ &= \int 1 - \exp\left[- \int \rho_i \left(a + \frac{b}{r_e} \right) \mathrm{d}z \right] \mathrm{d}y. \end{aligned} \tag{35}$$

We now focus on the influence of ice crystal distribution on extinction. For simplicity, let us assume a uniform distribution of ice crystals in a rectangle of area S and height h. The attenuation coefficient μ is then uniform in this rectangle. We then have

$$E(h, \mu, S) = \frac{S}{h}(1 - \mathrm{e}^{-\mu h}). \tag{36}$$

For given μ and S we have

$$\frac{\partial E}{\partial h} = -\frac{S}{h^2}(1 - \mathrm{e}^{-h\mu} + \mu h \mathrm{e}^{-h\mu}) < 0. \tag{37}$$

The extinction is then a decreasing function of the height of the rectangle: the more the cloud is extended horizontally, the greater the extinction. Nevertheless, given that $\mu h \ll 1$, $E = S\mu - Sh\mu^2/2$, so at first order it is the ice mass and crystal radius that determine the extinction.

B. Analysis

The influence of stratification and vortex to jet distance on plume total extinction for $RH_i = 140\%$ at $t = 5$ is shown in Fig. 11(a). The possible parameter regions for several aircraft are also indicated. The total extinction calculation requires the transform of the variables into physical units. The reference values used for this are $b_0 = 50.9\,\mathrm{m}$ (B777) and $\tau_0 = 27.6\,\mathrm{s}$ (see Table III). We find that the total extinction remains low when Fr^{-1} is small. This corresponds to two possible and distinct situations. The first is when the plume is initially close enough to the vortex. The required proximity to the vortex is all the more strict as stratification is stronger. In this case, the plume descends, and this leads to a weak and very local formation of ice crystals. As a result, the optical thickness has a reduced support and reaches small values, which leads to a low total extinction. This regime is illustrated by the cases $\mathrm{Fr}^{-1} = 0.2$ and $\bar{b}_{\mathrm{jet}}$ set to 0.31 and 0.79 in Fig. 12 that displays the spatial distribution of the attenuation coefficient for three stratification rates and three jet-to-vortex spacings.

The second situation is when the distance between the jets and the vortices is large (e.g., for $\mathrm{Fr}^{-1} = 0.2$ and $\bar{b}_{\mathrm{jet}} = 0.16$). In this case a part of the plume stretches vertically along the symmetry axis above the primary vortices. However, the extent of the plume is reduced in the horizontal direction and thus the total extinction remains low.

Conversely, total extinction is high when stratification is strong and the engine is initially not too close to the vortices. This region actually breaks into two subregimes, depending on the flow dynamics (see Fig. 9). In the first subregion a primary and a secondary wake coexist, e.g., $\mathrm{Fr}^{-1} = 1$ and $\bar{b}_{\mathrm{jet}}$ equal to 0.16 or 0.31. As the plume is not close to the vortex core it rises towards the secondary wake (see the right panel of Fig. 12). This results in a large optical thickness both at the symmetry axis where ice mass is important, and more widely in the horizontal extent of the secondary wake where the low temperature allows crystals to persist. In the second, e.g., $\mathrm{Fr}^{-1} = 1.4$ and $\bar{b}_{\mathrm{jet}} = 0.16$ or 0.31, the entire wake is present at flight altitude, but the fairly large distance between the plume and the center of the vortices allows it to extend horizontally, resulting in a widely distributed attenuation coefficient. So does the optical thickness, leading to a high total extinction.

Finally, when the stratification is very strong and the plume lies initially close to the vortices, e.g., $\mathrm{Fr}^{-1} = 1.4$ and $\bar{b}_{\mathrm{jet}} = 0.79$, the ice remains inside the vortices, as in the weakly stratified case, but this time at flight altitude. Due to lower temperatures at this higher altitude, optical thickness and thus total extinction are slightly higher than in the weakly stratified case.

To test the dependence of this plot on relative humidity, number of soot, and emission indices, we also calculate the total extinction for other values of these parameters. Figure 11(b) is obtained by keeping the same dimensionalization but taking a relative humidity of $RH_i = 120\%$. The distribution remains the same, but the values are lower, which results from the reduction of the amount of available water. In Fig. 11(c) it is assumed that only half of the soot are nucleation sites (or that the engine emits half as much soot), at $RH_i = 140\%$ (see [42] for a justification of the consistency of such a assumption). Similarly, the total extinction retains the same distribution but decreases significantly, which is to be expected considering the increase of the effective radii. The use of the emission indices and heat of combustion of a liquid hydrogen engine for $RH_i = 140\%$ in Fig. 11(d) shows a strong increase of the total extinction but again a pattern which does not vary in comparison to a usual kerosene engine. In conclusion, this sensitivity analysis shows that the evolution of total extinction upon stratification and jet position results essentially from the wake dynamics. However, the particular situation of the thermodynamic state of the atmosphere and engine type have a decisive impact on the amplitude of the total extinction. Hydrogen appears to cause the largest increase among all tests.

C. Wake roll-up and jet temperature influence on optical properties

In order to verify that the assumption of complete vortex roll-up is not too restrictive, the wake evolution is also calculated with a vorticity sheet representing the flow just behind the elliptical

charge as the initial velocity field. The vorticity sheet is initialized so that the resulting vortices have the same spacing and circulation as the Lamb-Oseen vortices of the general case. Figure 13 compares values of the total extinction of the plume as a function of Fr^{-1} when either taking into account the vorticity sheet roll-up or neglecting it. Only minor differences are found due to the roll-up of the vortex sheet. In conclusion, the initialization of the simulations with two Lamb-Oseen vortices is sufficient for objectives of the present investigation.

Figure 13 also considers the influence of jet temperature at the start of the vortex phase. It can be seen that doubling the temperature only marginally modifies the extinction, merely slightly reinforcing the dependence on b_{jet} by accentuating the extreme values on either side of the threshold.

V. CONCLUSION

A bidimensional parametric study on the effects of stratification and engine jet position along the wingspan is carried out to evaluate the potential radiative impact of early contrails during the vortex phase. This phase has the particularity of exhibiting a purely 2D dynamic. It has a particular role in the vertical dispersion of contrails due to the combined effects of stratification and jet-vortex interaction. A model is implemented in a normalized framework to account for the general behavior of the wake flow containing the contrails under these effects. The positions of the jets investigated range from the plane of symmetry of the aircraft to the wing tip. All possible values of stable stratification at flight altitudes are analyzed. Condensation is taken into account to assess the spatial distribution of ice mass and crystal radius and to describe the optical properties of the simulated contrails. This serves as a gauge to examine the radiative impact of the possibly formed cloud as a function of the initial wake and atmospheric properties. It must be denoted that the normalization approach taken here makes the present study a large multidimensional analysis that encompasses the aerodynamic properties of the aircraft and the stratification of the atmosphere. The atmospheric stratification in itself is not enough as the behavior depends on the effective stratification which also accounts for the wake and, indirectly, the aircraft. A return to the physical units is performed for a selection of aircraft to provide real life diagnostics. This return requires some hypothesis on ice condensation.

The more important thing that we neglect is the influence of phase change over the temperature field (that is latent heat of sublimation). In the same way, the computation of the microphysics of the plume (chemistry of the condensation over soot, homogeneous nucleation, nonimmediate condensation, and crystal growth) is neglected. By design, the model cannot take these improvements into account. Indeed, considering them would mean giving up the normalization of the entire problem by a small number of parameters that is applied here and would therefore prevent the parametric study. More constrained parametric studies have been realized [12,13,21,26] with the use of more advanced plume model, and selected parameters variations, but they do not provide the basis for studying the issue as a standardized problem.

Important results are found regarding the effects of stratification and jet position along the wing. Three main behaviors are observed. For low levels of stratification, the ice plume descends with the wake vortices, generating a small optical impact. This impact is smaller the closer the jets are to the wing tip vortices. For high levels of stratification and small jet spacing, the ice plume tends to remain at the flight altitude and to expand horizontally, generating a higher optical impact. The boundary between these two regimes is quite clear and lies at a threshold that depends on time, for instance, $\mathrm{Fr}^{-1} = 0.75\,\bar{b}_{\mathrm{jet}} + 0.45$ for $t = 5\,\tau_0$. It results from the wake dynamics and is also observable examining the altitude of the plume. In a nutshell, the plume is found at flight altitude (in the secondary wake) for high levels of stratification and small jet spacing, and at a lower altitude (in the primary wake) for lower levels of stratification. At the threshold, the plume is present in both the primary and secondary wake, as well as near the symmetry axis. This generates a larger optical impact than when it remains in the primary wake, but less than when it rises in the secondary wake. Finally, for high values of stratification and jet spacing, the plume remains concentrated in the

vortices at flight altitude, resulting in low optical impact. A comparison with the possible parameter ranges for current twin-engine aircraft shows that in most cases the ice plume is no longer present in the vortices at the end of the vortex phase. This dynamic is totally realistic, and in particular is not the consequence of the 2D approximation, even if the description of the evolution of the secondary wake at flight altitude is distorted by the turbulence that develops there. A comparison with a 3D simulation confirms that the dynamics of the primary wake, and thus the vertical motion of the vortex dipole, and the entrainment of the plume by one or the other wake, and thus the evolution of its altitude, are intrinsically 2D mechanisms. Taking into account the vortex roll-up shows that it has little impact on the results. Importantly, these results indicate the large variability of the contrail appearance depending on the atmospheric conditions but also on the specific aircraft configuration (wing-jet configuration and weight). In general, contrails do not lie with the primary vortices but with the secondary wake, between the flight altitude and the altitude of the vortices, or even at flight altitude. For an observer present at the ground or for automatic observation of contrails (by means of satellites or ground cameras), this sensitivity of the contrail properties must be taken into account to correlate well the relations between contrail, aircraft and atmosphere. Overall this shows that the near wake dynamics has a profound influence on the contrail issue. The parameters related to condensation (emission indices, heat of combustion, and relative humidity) have an influence on the amount of ice produced and thus on the optical impact of the wake. However, these parameters have no influence on the dependence of these properties on the stratification and the lateral position of the jet. The results obtained are essentially dependent on the dynamics of the wake and in this sense are applicable to a large number of situations, in particular to different atmospheric or propulsion situations. For current aircraft, the total extinction of contrails, which is a measure of their optical impact, can be low or high. Among other things, these variations are dependent on the weight of the aircraft and stratification of the atmosphere, parameters that cannot be modified. Therefore, the effect of jet spacing is of particular interest as it could be used as a contrail mitigation strategy. From a purely aerodynamic point of view, placing the jet close to the location of the rolled-up vortex ($\bar{b}_{\text{jet}} \simeq 0.8$) is on average beneficial to reduce total extinction and is not far off from the most outboard engines of current four-engine aircraft.

ACKNOWLEDGMENTS

This work has been supported by the French Ministry of Civil Aviation (DGAC, 100020995) under the Climaviation research program. The authors thank Herman Mak for his valuable help with the English wording.

[1] D. S. Lee, D. W. Fahey, A. Skowron, M. R. Allen, U. Burkhardt, Q. Chen, S. J. Doherty, S. Freeman, P. M. Forster, and J. Fuglestvedt, The contribution of global aviation to anthropogenic climate forcing for 2000 to 2018, Atmos. Environ. **244**, 117834 (2021).

[2] H. Appleman, The formation of exhaust condensation trails by jet aircraft, Bull. Am. Meteorol. Soc. **34**, 14 (1953).

[3] U. Schumann, On conditions for contrail formation from aircraft exhausts, Meteorol. Z. **5**, 4 (1996).

[4] L. Jacquin and F. Garnier, On the dynamics of engine jets behind a transport aircraft (ONERA-Publications-TP, Meudon, 1996).

[5] T. Gerz, T. Dürbeck, and P. Konopka, Transport and effective diffusion of aircraft emissions, J. Geophys. Res.: Atmos. **103**, 25905 (1998).

[6] R. Paoli and K. Shariff, Contrail modeling and simulation, Annu. Rev. Fluid Mech. **48**, 393 (2016).

[7] P. G. Saffman, *Vortex Dynamics* (Cambridge University Press, Cambridge, 1993).

[8] S. Unterstrasser, Properties of young contrails–a parametrisation based on large-eddy simulations, Atmos. Chem. Phys. **16**, 2059 (2016).

[9] F. Garnier, L. Jacquin, and S. Brunet, Numerical/experimental simulation of exhaust jet mixing in wake vortex, in *30th Fluid Dynamics Conference, Norfolk, VA, USA*, paper No. AIAA 1999-3418 (AIAA, 1999).
[10] L. Jacquin, P. Molton, P. Loiret, and E. Coustols, An experiment on jet-wake vortex interaction, in *37th AIAA Fluid Dynamics Conference and Exhibit, Miami, Florida*, paper No. AIAA 2007-4363 (AIAA, 2007).
[11] R. Paoli, F. Laporte, B. Cuenot, and T. Poinsot, Dynamics and mixing in jet/vortex interactions, Phys. Fluids **15**, 1843 (2003).
[12] S. Unterstrasser, K. Gierens, and P. Spichtinger, The evolution of contrail microphysics in the vortex phase, Meteorol. Z. **17**, 145 (2008).
[13] S. Unterstrasser, Large-eddy simulation study of contrail microphysics and geometry during the vortex phase and consequences on contrail-to-cirrus transition, J. Geophys. Res.: Atmos. **119**, 7537 (2014).
[14] R. Paoli, L. Nybelen, J. Picot, and D. Cariolle, Effects of jet/vortex interaction on contrail formation in supersaturated conditions, Phys. Fluids **25**, 053305 (2013).
[15] F. Garnier, S. Brunet, and L. Jacquin, Modelling exhaust plume mixing in the near field of an aircraft, Ann. Geophys. **15**, 1468 (1997).
[16] J.-C. Khou, W. Ghedhaïfi, X. Vancassel, and F. Garnier, Spatial simulation of contrail formation in near-field of commercial aircraft, J. Aircr. **52**, 1927 (2015).
[17] D. Kolomenskiy and R. Paoli, Numerical simulation of the wake of an airliner, J. Aircr. **55**, 1689 (2018).
[18] P. R. Spalart, Airplane trailing vortices, Annu. Rev. Fluid Mech. **30**, 107 (1998).
[19] S. C. Crow, Stability theory for a pair of trailing vortices, AIAA J. **8**, 2172 (1970).
[20] S. C. Crow and E. R. Bate, Lifespan of trailing vortices in a turbulent atmosphere, J. Aircr. **13**, 476 (1976).
[21] D. Lewellen and W. Lewellen, The effects of aircraft wake dynamics on contrail development, J. Atmos. Sci. **58**, 390 (2001).
[22] T. Sarpkaya, Trailing vortices in homogeneous and density-stratified media, J. Fluid Mech. **136**, 85 (1983).
[23] R. S. Scorer and L. J. Davenport, Contrails and aircraft downwash, J. Fluid Mech. **43**, 451 (1970).
[24] A. A. Shirgaonkar and S. K. Lele, Interaction of vortex wakes and buoyant jets: A study of two-dimensional dynamics, Phys. Fluids **19**, 086601 (2007).
[25] P. R. Spalart, On the motion of laminar wing wakes in a stratified fluid, J. Fluid Mech. **327**, 139 (1996).
[26] S. Unterstrasser, R. Paoli, I. Sölch, C. Kühnlein, and T. Gerz, Dimension of aircraft exhaust plumes at cruise conditions: Effect of wake vortices, Atmos. Chem. Phys. **14**, 2713 (2014).
[27] S. Unterstrasser and N. Görsch, Aircraft-type dependency of contrail evolution, J. Geophys. Res.: Atmos. **119**, 14,015 (2014).
[28] D. Papamoschou and A. Roshko, The compressible turbulent shear layer: An experimental study, J. Fluid Mech. **197**, 453 (1988).
[29] S. Chandrasekhar, *Hydrodynamic and Hydromagnetic Stability*, Smithsonian Miscellaneous Collections (Dover, New-York, 1981) first printed by Clarendon Press (1961).
[30] R. J. List, *Smithsonian Meteorological Tables*, 6th rev. ed., Vol. 114 (Smithsonian Institution Press, Washington, DC, 1951).
[31] G. K. Vallis, D. J. Parker, and S. M. Tobias, A simple system for moist convection: The Rainy–Bénard model, J. Fluid Mech. **862**, 162 (2019).
[32] W. L. Flower, Measurements of the diffusion coefficient for soot particles in flames, Phys. Rev. Lett. **51**, 2287 (1983).
[33] C. C. Wey, B. E. Anderson, C. Wey, R. C. Miake-Lye, P. Whitefield, and R. Howard, Overview on the aircraft particle emissions experiment (APEX), J. Propul. Power **23**, 898 (2007).
[34] C. Cambon, J.-P. Benoit, L. Shao, and L. Jacquin, Stability analysis and large-eddy simulation of rotating turbulence with organized eddies, J. Fluid Mech. **278**, 175 (1994).
[35] S. P. Govindaraju and P. G. Saffman, Flow in a turbulent trailing vortex, Phys. Fluids **14**, 2074 (1971).

[36] T. Gerz, F. Holzäpfel, and D. Darracq, Commercial aircraft wake vortices, Prog. Aerosp. Sci. **38**, 181 (2002).
[37] U. Schumann, A contrail cirrus prediction model, Geosci. Model Dev. **5**, 543 (2012).
[38] E. E. Ebert and J. A. Curry, A parameterization of ice cloud optical properties for climate models, J. Geophys. Res.: Atmos. **97**, 3831 (1992).
[39] S. Unterstrasser and K. Gierens, Numerical simulations of contrail-to-cirrus transition—Part 1: An extensive parametric study, Atmos. Chem. Phys. **10**, 2017 (2010).
[40] S. E. Widnall, The structure and dynamics of vortex filaments, Annu. Rev. Fluid Mech. **7**, 141 (1975).
[41] J. F. Garten, S. Arendt, D. C. Fritts, and J. Werne, Dynamics of counter-rotating vortex pairs in stratified and sheared environments, J. Fluid Mech. **361**, 189 (1998).
[42] T. Bräuer, C. Voigt, D. Sauer, S. Kaufmann, V. Hahn, M. Scheibe, H. Schlager, F. Huber, P. Le Clercq, R. H. Moore, and B. E. Anderson, Reduced ice number concentrations in contrails from low-aromatic biofuel blends, Atmos. Chem. Phys. **21**, 16817 (2021).